Journal of Cleaner Production 278 (2021) 123933

Contents lists available at ScienceDirect

Journal of Cleaner Production

journal homepage: www.elsevier.com/locate/jclepro

Phosphorus removal from aqueous solutions by adsorptive concrete aggregates

Fan Wu [a, b, c], Qingliang Yu [a, d, *], F. Gauvin [a], H.J.H. Brouwers [a], Changwu Liu [b, c, e, **]

[a] Department of the Built Environment, Eindhoven University of Technology, P.O. Box 513, 5600 MB, Eindhoven, the Netherlands
[b] Institute of Disaster Management and Reconstruction, Sichuan University-The Hong Kong Polytechnic University, No.1Huanghe Road, Chengdu, 610065, PR China
[c] College of Water Resource and Hydropower, Sichuan University, No.24 South Section 1, Yihuan Road, Chengdu, 610065, PR China
[d] School of Civil Engineering, Wuhan University, No.299 Bayi Road, Wuchang District, Wuhan, 430072, PR China
[e] State Key Laboratory of Hydraulics and Mountain River Engineering, Sichuan University, No.24 South Section 1, Yihuan Road, Chengdu, 610065, PR China

ARTICLE INFO

Article history:
Received 14 April 2020
Received in revised form
24 July 2020
Accepted 22 August 2020
Available online 28 August 2020

Handling editor. Cecilia Maria Villas Bôas de Almeida

Keywords:
Phosphorus removal
Steel slag
Expanded silica
Miscanthus
Peach shell
Adsorption kinetics

ABSTRACT

The purpose of this study is to investigate the adsorption characteristics of granular aggregates under identical experimental conditions for potential applications in highly adsorptive concrete. In this study, industrial by-products (steel slag), lightweight aggregates (expanded silica) and bio-materials (peach shell and miscanthus) are used for phosphorus (P) removal from aqueous solutions. The effects of several parameters such as the initial concentrations of P, reaction time and pH value on adsorption capacity and efficiency of P are investigated using an IC analyzer. Results show that the phosphorus adsorption of all absorbents follows the adsorption isotherms with a varying phosphorus concentration from 5 mg/L to 700 mg/L, and the adsorption isotherms data are fitted well by Langmuir equation. The steel slag exhibits a higher P-adsorption capacity and adsorption efficiency compared to lightweight aggregates and bio-materials, with an estimated maximum adsorption capacity by steel slag of 20.4 mg/g. Moreover, the P-desorption results show that steel slag has a very low P-desorption. Heat treatment is used to increase the adsorption capacity of the miscanthus owing to the change in pore structure characteristics determined by BET. The adsorption kinetic data of the steel slag follows a pseudo-second-order model. The ICP-AES, XRD and SEM-EDS analyses show that the P-adsorption of the miscanthus and peach shell follows physical adsorption, whereas the adsorption mechanism of the steel slag can be attributed to the Ca^{2+} released from the steel slag, which can react with P and form a stable Ca–P precipitate. It is suggested that steel slags can function as effective adsorptive aggregate for the manufacture of highly adsorptive concrete.

1. Introduction

The development of urbanization leads to an increasing impact of human activities on aqueous environments (Gizińska-Górna et al., 2017). Stormwater runoff from urban catchment areas is one of the biggest sources of water pollution (Bannerman et al., 1993). During the rainy season, the pollutants on road surfaces such as heavy metals, pesticides and organic contaminants etc. are entrained into the stormwater and flow into the nearest water body (Wang et al., 2018), which pose a huge threat to ecological safety and public health (Rizzo and Rizzo, 2015). Among these pollutants, phosphorus (P) is one of the main pollutants from stormwater runoff (Park et al., 2017; Zhu et al., 2018). In extreme conditions, the excess supply of P causes the eutrophication and excessive algal blooms, which leads to the degradation of water quality, and the mortality of fish and aquatic plants (Guo et al., 2018). Therefore, it is vital to remove the P from stormwater before they are discharged into the water body.

In recent years, ordinary pervious concrete has been used for pollutants removal from stormwater runoff. Shabalala et al. (2017) reported that pervious concrete can remove more than 75% of the heavy metals from acid mine drainage. Jo et al. (2015) investigated

* Corresponding author. Department of the Built Environment, Eindhoven University of Technology, P.O. Box 513, 5600 MB, Eindhoven, the Netherlands.
** Corresponding author. College of Water Resource and Hydropower, Sichuan University, No.1Huanghe Road, Chengdu, 610065, PR China.
E-mail addresses: q.yu@bwk.tue.nl (Q. Yu), liuchangwu@scu.edu.cn (C. Liu).

https://doi.org/10.1016/j.jclepro.2020.123933

Abbreviations

A_e	Adsorption removal capacity (mg/g)
A_t	Amount of P adsorbed by the adsorbent at any time (mg/L)
C	P concentration in the solution (mg/L)
C_0	Initial P concentration (mg/L)
C_e	P concentration in the solution at equilibrium (mg/L)
ES	Expanded silica
K_1	Rate constant of Lagergren pseudo-first-order kinetic models
K_2	Rate constant of Lagergren pseudo-second-order kinetic models
K_L	Adsorption constant in Langmuir isotherm
K_F	Constant of Freundlich isotherm
M	Miscanthus
M-3hour	Heat-treated miscanthus for 3 h
N	Heterogeneity factor of Freundlich isotherm
Q_m	Maximum adsorption capacity in Langmuir isotherm
P_d	P-desorption rate (%)
P_R	P-removal rate (%)
PS	Peach shell
Q	P-adsorption capacity(mg/g)
q_d	P-desorption capacity (mg/g)
SS	Steel slag
T_P	P content in the P-saturated sample
V	Volume of solution (L)

the use of fly ash geopolymer paste in pervious concrete for the removal of faecal coliforms and P and the average removal of faecal coliforms and P are 43.1% and 21.9%, respectively. Rivera et al. (2015) studied that the addition of fly ash and iron oxide nanoparticles in pervious concrete improves P removal. The adsorption capacity of different pervious concrete for pollutants removal is summarized in Table 1. The adsorption capacity of ordinary pervious concrete is very limited because gravel or sand without adsorption capacity is used as aggregates in ordinary pervious concrete. Moreover, a very long contact time is often required, even at a low initial pollutant concentration (Haselbach et al., 2014). Therefore, in order to improve the adsorption capacity of ordinary pervious concrete, a potentially effective method is to replace non-adsorptive aggregates with high adsorptive aggregates.

Currently, various methods such as ion exchange, chemical precipitation, biological processes and physical adsorption, etc. have been used for P removal from the aqueous environment (Naghipour et al., 2015). With the requirements of sustainable development, different low-cost and high-adsorption materials are gradually employed for wastewater treatment, such as fly ash (Agyei et al., 2002), pumice (Taylor et al., 2014), steel slag (Barca et al., 2014; Bowden et al., 2009), lightweight expanded materials (Forbes et al., 2004; Nkansah et al., 2012), peach shell (PS) (Dastgheib and Rockstraw, 2001), miscanthus (M) (Osman et al., 2018), plantage ovata (Yaghoobi et al., 2017), etc. Although most of these materials show good adsorption characteristics, they are not suitable as adsorptive concrete aggregates considering size and strength requirements. Besides, most of the current studies mainly focus on the adsorption capacity of powdery materials. The adsorption capacity of the low-cost, available and high adsorptive aggregates for the manufacture of highly adsorptive concrete should be evaluated by granular aggregate rather than powder.

Steel slag (SS) is a by-product from the steel industry, which has been widely used as an aggregate and a cement component for construction and building materials. The main dominant components of the SS are calcium oxide (CaO) and iron oxide (Fe_2O_3), which are the result of the addition of the fluxing agent during the steelmaking process (Barca et al., 2012). The high content of metal oxide makes it a potential adsorbent, and it has attracted more attention to remove P from wastewater (Park et al., 2017; Shilton et al., 2006). The release of calcium ions (Ca^{2+}) from the SS that can be combined with phosphorus ions (PO_4^{3-}) by Ca–P precipitation-coagulation mechanism (Bowden et al., 2009). More than 50% of the SS is composed of calcium-containing minerals (Shi, 2004), indicating sufficient calcium ions can be supplied for the precipitation-coagulation process. Porous lightweight aggregates also can be used to remove the heavy metals and organic pollutants from wastewater due to the well-developed pore structure (Lee et al., 2011; Sayari et al., 2005). Adsorptive aggregates should be low-cost, eco-friendly and available, thus bio-based aggregates (PS, M, etc.) may be feasible for recyclable adsorptive materials for pollutant removal. Although these materials are potential adsorptive aggregates that can be used for the manufacture of high adsorptive concrete, different experimental conditions affect the physico-chemical properties of materials, even the same material exhibits different adsorption capacities with varying conditions such as initial concentration, reaction time, pH, temperature and agitation mode, etc (Barca et al., 2012). Therefore, a direct comparison of the adsorption capacity of these materials is not feasible (Park et al., 2017). The adsorption properties of different adsorptive aggregates under identical experimental condition should be investigated and the optimized aggregates for potential application in highly adsorptive concrete should be obtained.

The purpose of this study was to investigate the adsorption characteristics of granular aggregates under identical experimental conditions for potential applications in highly adsorptive concrete. The industrial by-products (SS), lightweight aggregates (expanded silica (ES)) and bio-materials (PS and M) were used for P removal from aqueous solutions. The effects of the initial concentration of P, reaction time and pH on the adsorption capacity and efficiency of P were investigated using an ion chromatography (IC) analyzer. The adsorption isotherms and adsorption kinetics models of P-

Table 1
Adsorption capacity of different pervious concrete for pollutants removal.

Types of concrete	Pollutants	Initial concentration	Removal capacity	Contact time	References
Pervious concrete	Cu, Co, Ni	0.1–1.3 mg/L	>75%	6 months	Shabalala et al. (2017)
Pervious concrete containing fly ash	P	2.58–3.4 mg/L	25–85%	0.5–8 h	Jo et al. (2015)
Pervious concrete containing iron oxide	P	10 mg/L	>90%	72 h	Vázquez-Rivera et al. (2015)
Ordinary pervious concrete	Cu & Zn	20 μm/L &100 μm/L	87% & 90%	10 cycles	Haselbach et al. (2014)
Ordinary Portland cement	P	400 mg/L	20.75%	–	Agyei et al. (2002)
Aluminium hydroxide-coated sand	P	25 mg/L	0.239 mg/g	24 h	Han et al. (2009)

absorption were derived. The pore structural properties of the materials were analyzed using Brunauer Emmett Teller (BET) method. The adsorption mechanism of phosphorus was discussed based on the results analyzed from inductively coupled plasma atomic emission spectroscopy (ICP-AES), X-ray diffraction (XRD) and scanning electron microscope combined with energy dispersive spectrometer (SEM-EDS).

2. Materials and methods

2.1. Materials

The steel slag (SS) (TATA Steel, The Netherlands), commercial expanded silica (ES), miscanthus (M) (NNRGY, The Netherlands) and commercial PS biochar are used as absorptive materials in this study. The heat-treated miscanthus (M-3hour) under nitrogen condition at 250 °C for 3 h is also used as an absorbent for comparison (Luo et al., 2013). All raw materials with a particle size of 1–2 mm are selected to investigate the adsorption performance of the granular aggregates. They are washed twice with distilled water to remove any contaminations, and then oven-dried at 105 °C for 24 h and stored in air-tight containers until the test.

The high content of metal oxides contributes to a strong affinity for P-adsorption (Kaasik et al., 2008). The chemical compositions of steel slag and expanded silica are determined by X-ray fluorescence spectroscopy (XRF), as presented in Table 2. The main chemical components of the SS are CaO (40.0%), Fe_2O_3 (31.5%) and SiO_2 (10.4%). The ES is mainly composed of SiO_2 (51.3%), Al_2O_3 (19.6%) and Na_2O (14.8%). The PS and M are organic matter, and their chemical compositions are mainly composed of C, H, O and N (Wu et al., 2018). The SEM images of the adsorbents are shown in Fig. 1. Many micropores are observed on the surface of the PS, ES and M-3hour (Fig. 1a, c and 1e). The SS displays a densified surface, but microscopic cracks with the width of smaller than 5 μm are observed on the surface (Fig. 1b). The internal surface of the M is parenchyma like cavity structure (Fig. 1d).

2.2. P-adsorption experiments

In this study, artificial P solution is prepared for the adsorption test. A stock P solution of 1000 mg/L is prepared by dissolving the chemically pure potassium dihydrogen phosphorus (KH_2PO_4) in distilled water. All standard P solutions with the desired concentration are prepared by diluting the stock P solution with distilled water.

2.2.1. Effect of different adsorbents on adsorption

A preliminary experiment is conducted to evaluate the adsorption capacity of different raw materials. 1 g of the adsorbent material is added to a 25 ml P solution with a concentration of 50 mg/L. The mixture is stirred at 225 rpm in the thermostatic shaker for 24 h and then is filtered by a 0.45 μm membrane. The extracted supernatant is used for the P concentration test.

The P-adsorption capacity (q, mg/g) and P-removal rate (P_R, %) are calculated as follows:

Table 2
Chemical compositions of steel slag and expanded silica (wt.%).

Oxides	CaO	SiO_2	Al_2O_3	Fe_2O_3	SO_3	MgO	K_2O	Na_2O	LOI
Steel slag	40.0	10.4	1.6	31.5	0.4	5.0	–	–	3.3
Expanded silica	1.0	51.3	19.6	2.6	0.5	–	6.2	14.8	2.7

$$q = \frac{C_0 - C_e}{M} \times V \quad (1)$$

$$P_R = \frac{C_0 - C_e}{C_0} \times 100\% \quad (2)$$

Where C_0 is the initial P concentration (mg/L), C_e is the P concentration in the solution at equilibrium (mg/L), M is the mass of sample (g), and V is the volume of solution (L).

2.2.2. Adsorption isotherms

The adsorption isotherms of P are evaluated by batch experiments. For the sorption isotherms, 1g of the adsorbent is loaded in 50 ml polyethene centrifuge tube and mixed with 25 ml of various P solution (5–700 mg/L). The flask is covered and stirred at 225 rpm for 24 h to ensure approximate equilibrium. After P adsorption, the solution is filtered through a 0.45 μm membrane filter and then analyzed for P concentration.

The Langmuir and Freundlich equations are used for analyzing the adsorption isotherms of adsorbents, as described below:

$$\text{Langmuir equation: } A_e = \frac{Q_m K_L C_e}{1 + K_L C_e} \quad (3)$$

$$\text{Freundlich equation: } A_e = K_F C_e^{\frac{1}{n}} \quad (4)$$

Where A_e is the adsorption removal capacity (mg/g), C_e is the P concentration in the solution at equilibrium (mg/L), Q_m is maximum adsorption capacity in Langmuir isotherm, K_L is adsorption constant in Langmuir isotherm, K_F is the constant of Freundlich isotherm, n is heterogeneity factor of Freundlich isotherm.

2.2.3. Adsorption kinetics

The adsorption kinetics experiments are performed using a procedure similar to the one used for the adsorption isotherm test. A series of bottles with 1g of adsorbent and 100 ml of solution with a set P concentration of 100 mg/L, then mixed and shaken for different contact time (0.25, 0.5, 1, 2, 4, 6, 8, 12, 16 and 24 h). The solution is filtered and determined for residual concentration.

The Lagergren pseudo-first-order equation, pseudo-second-order equation and simple Elovich equation are used for describing the adsorption kinetics of adsorbents in this study:

$$\text{Pseudo} - \text{first} - \text{order equation: } \frac{dA_t}{dt} = k_1(A_e - A_t) \quad (5)$$

$$\text{Pseudo} - \text{second} - \text{order equation: } \frac{dA_t}{dt} = k_2(A_e - A_t)^2 \quad (6)$$

$$\text{Simple Elovich equation: } q = \alpha + \beta \ln t \quad (7)$$

Where A_t is the amount of P adsorbed by the adsorbent at any time (mg/L), A_e is the adsorption removal capacity (mg/g), K_1 and K_2 is the rate constant of Lagergren pseudo-first-order and pseudo-second-order kinetic models.

2.2.4. Effects of pH on adsorption capacity

The effects of pH on P-adsorption are determined by a series of experiments with constant initial P concentration (100 mg/L) and adsorbent dosage (1g) and various pH values (3, 5, 7, 9 and 11). 1M NaOH and 0.5 M HCl are used to adjust the pH value of the tested P solution.

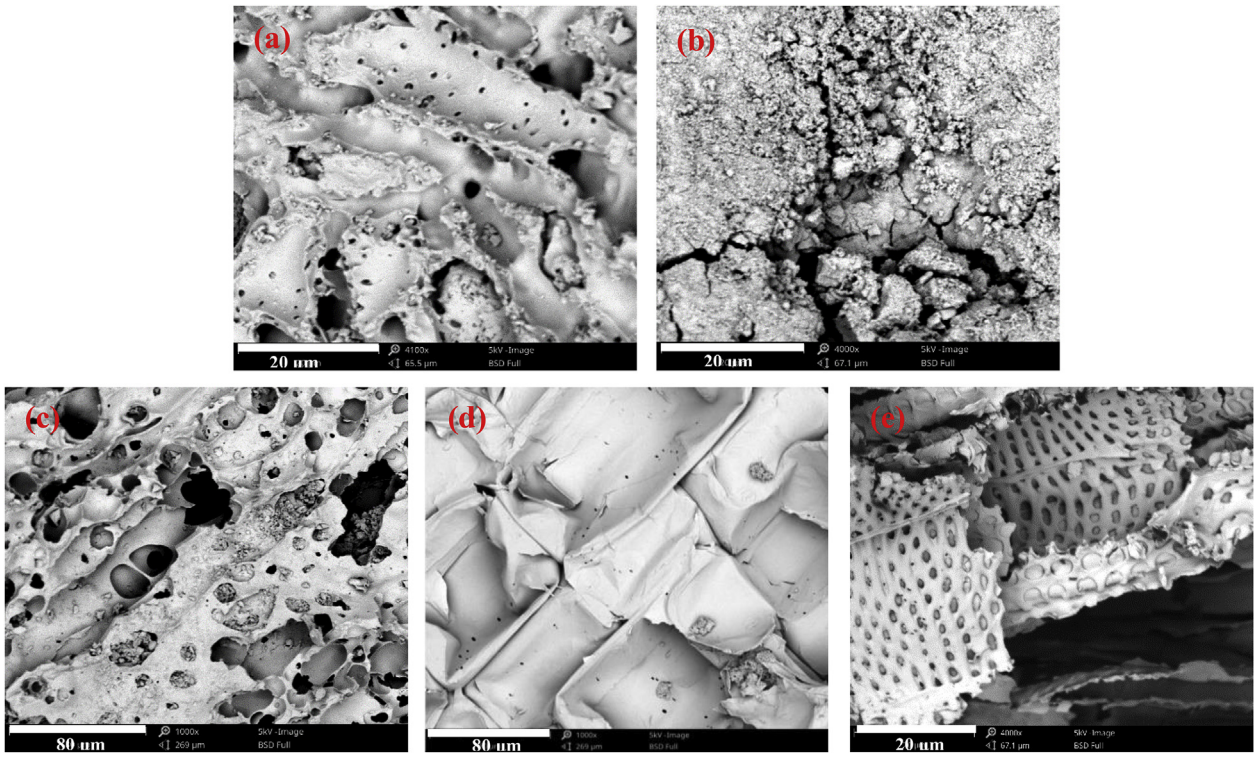

Fig. 1. SEM images of (a) PS, (b) SS, (c) ES, (d) M and (e) M-3hour.

2.3. P-desorption experiments

P-saturated adsorbent (1g) with 50 mg/L P-solution is placed in a 50 ml tube with 25 ml distilled water. After that, the tube is continuously shaken in a shaker at 225 rpm for 24 h. The mixture is centrifuged and filtered, and the P is determined by the same method described above. P-desorption capacity (q_d, mg/g) is calculated:

$$q_d = \frac{CV}{M} \tag{8}$$

The P-desorption rate (P_d) is calculated:

$$P_d = \frac{CV}{T_P} \times 100\% \tag{9}$$

where C is the P concentration in the solution (mg/L), M is the mass of sample(g), V is the volume of the solution(L), and T_P is the P content in the P-saturated sample.

2.4. Analytical methods

The microstructural properties of all samples including BET-surface area, pore volume and pore size are determined by nitrogen adsorption/desorption test. The mineralogical composition of all samples before and after absorption of P is determined by XRD. The microstructure of all samples before and after the test is observed by SEM-EDS. Before SEM-EDS analysis, all samples are coated with Au. Metal ions such as calcium (Ca^{2+}), iron (Fe^{2+}), magnesium (Mg^{2+}), etc. are measured through ICP-AES. The concentration of P is analyzed by IC.

3. Results and discussion

3.1. Pore structure of materials

The P-adsorption capacity depends on the differences in chemical composition, microstructure, and pore characteristics (Jiang et al., 2014). Most of powders or aggregates such as clay, pigment, cement exhibited Type II isotherms, and the narrow hysteresis loop is generated by inter-particle capillary condensation (Rouquerol et al., 2013). As shown in Fig. 2, the adsorption-desorption isotherm curves of all materials belonged to the Type II isotherms based on the International Union of Pure and Applied Chemistry (IUPAC) classification (Rouquerol et al., 2013). Moreover, a narrow hysteresis loop is observed in the adsorption-desorption isotherms curve, which indicates that the micropores and mesopores are well developed (Jung et al., 2015; Lin et al., 2016). The results also show that the PS adsorbed more nitrogen than other materials under the same relative pressure conditions, which indicates that the PS has more developed pore structures.

The pore size of adsorbents can be divided into micropores (<2 nm), mesopores (2−50 nm) and macropores (>50 nm) (Zhang and Li, 2011). The pore size distribution of the material is estimated by the Barrett-Joyner-Halenda (BJH) method from the desorption data of BET test, as shown in Fig. 3. The pore structure properties of the material are shown in Table 3. As shown in Fig. 3, most of the pores of the PS and SS are less than 10 nm, which indicates that they may have better adsorption capacity compared to the ES and the M. Generally, the mesopores mainly play the role of the channel for the solution to enter the interior of the PS. The most of pore volume of the ES and M is less than 50 nm, and they are in the range of mesopores. The cumulative pore volume of the M and M-3hour are 0.0088 cm^3/g and 0.0073 cm^3/g, respectively, which indicates that the heat treatment reduces the pore volume and pore size of the M,

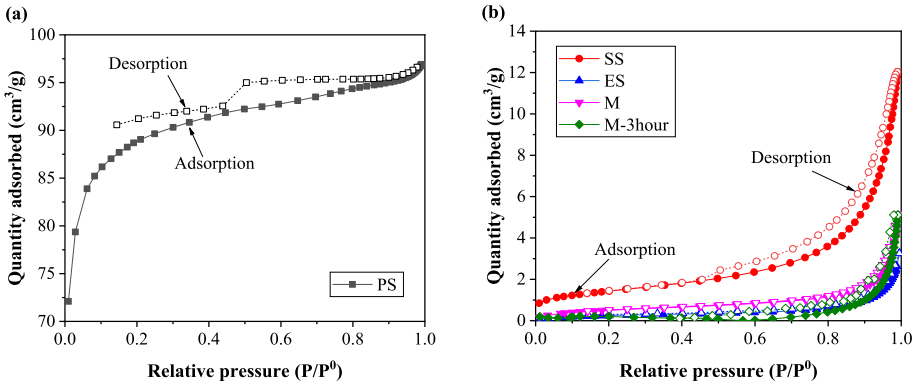

Fig. 2. The nitrogen adsorption-desorption isotherms of the material.

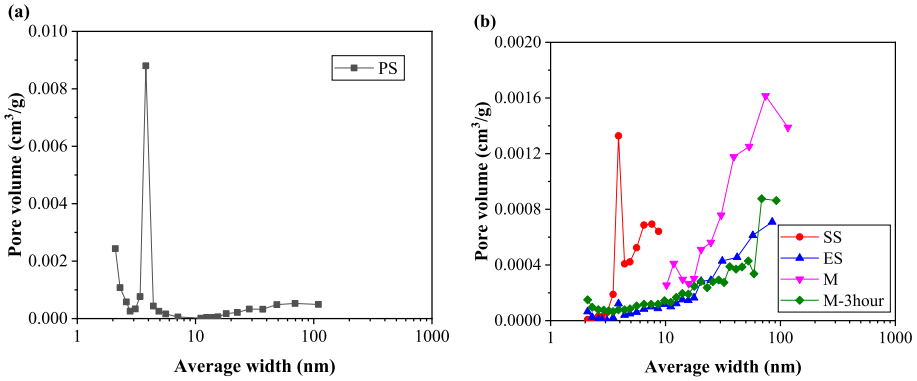

Fig. 3. The Barrett-Joyner-Halenda (BJH) pore size distribution of the material.

Table 3
Physical properties of materials.

Materials	BET surface area (m^2/g)	Micropore area (m^2/g)	Pore size (nm)	Pore volume (cm^3/g)
Peach shell (PS)	297.4	237.3	2.01	0.1494
Steal slag (SS)	5.14	0.58	13.18	0.0017
Expanded silica (ES)	1.03	0.07	14.49	0.0037
Miscanthus (M)	0.12	0.54	30.66	0.0066
Heat-treated miscanthus (M-3hour)	1.98	1.40	12.75	0.0063

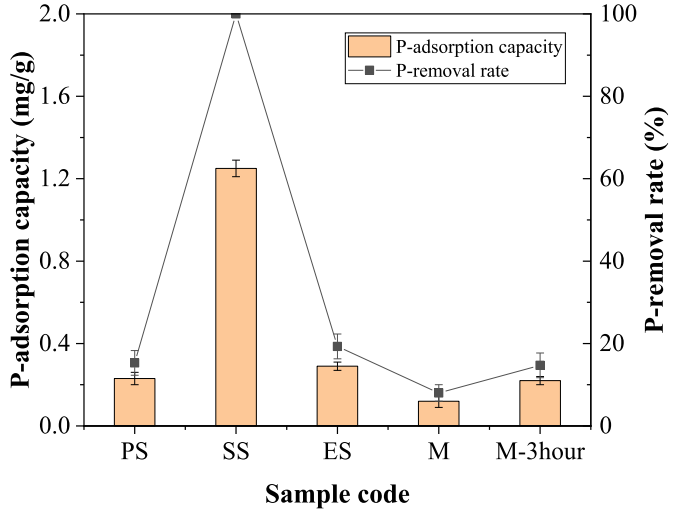

Fig. 4. The P removal capacity and rate of the material in the P solution of 50 mg/L(Adsorbent: 1g, P solution volume: 25 ml, Revolution per minute: 225, Time: 24 h).

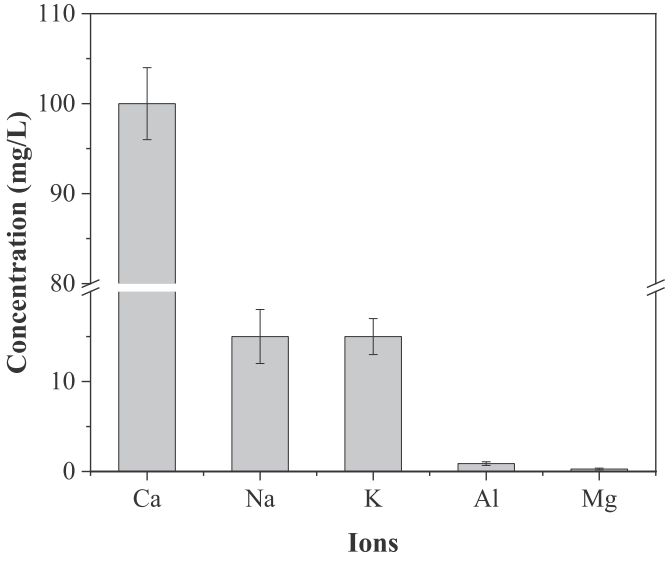

Fig. 5. The ions released from steel slag.

consequently increasing the specific surface area, as shown in Table 3. Therefore, the M-3hour may have better uptake of P because of the well-developed mesoporous structure and high specific surface area compared to the untreated M (Luo et al., 2013).

3.2. P-adsorption

3.2.1. Effect of different materials on adsorption

The P removal capacity and removal rate of the material after 24 h in P solution of 50 mg/L are shown in Fig. 4. The results show that the SS and ES have a higher capacity for P removal compared with other bio-materials. The P-removal rate of the SS is 100%, while the adsorption capacity of other materials for P removal is very limited, with a range of 8%–19%. The high P adsorption capacity of the SS is attributed to the calcium ions leached from the SS surface, which can be bound with P ions in the solution to form a stable precipitate (Jiang et al., 2014; Yin et al., 2011).

The ions release from the SS surface are presented in Fig. 5. Some metals ions such as K, Na and Mg ions do not significantly affect the P-adsorption capacity (Helyar et al., 1976a, 1976b), whereas metal ions (i.e. Ca, Fe, Al) released from the materials have a strong affinity with P. Previous studies have reported that the relative effects of the different cations on P-adsorption capacity (Helyar et al., 1976a), with the order of Ca > Mg > K > Na (Lehr and Van Wesemael, 1952). Hence, among the metal ions, the Ca^{2+} concentration is one of the key parameters for the Ca–P precipitation (Barca et al., 2012), the adsorption process is shown in Fig. 6a. Although sodium ions are also leached from the solution of the SS, the sodium ions have no significant effect on the adsorption of P, as reported by Bowden et al. (2009) and Yin et al. (2011). For the SS, the P-removal capacity is dominated by a chemical process, a large amount of calcium ions leach from the SS surface supply enough dissolved calcium ions to the solution and react with P and precipitate in the form of hydroxyapatite following the chemical reactions (Barca et al., 2012; Park et al., 2017):

$$CaO + H_2O \rightarrow Ca^{2+} + 2OH^- \quad (10)$$

$$5Ca^{2+} + 3PO_4^{3-} + OH^- \rightarrow Ca_5(PO_4)_3(OH)\downarrow \quad (11)$$

However, the PS and M are organic matter, which are mainly composed of C, N and O elements, indicating that the P-removal is achieved by pore-filling and electrostatic attraction (Tan et al., 2015), as shown in Fig. 6b. The high specific surface area and more mesoporous structure are crucial for improving the uptake capacity of P (Jung et al., 2015). The results confirm that the M-3hour increases the adsorption capacity compared to the M. Previous researches show that the bio-materials made from bamboo, maize residue and soybean stover have a low P-removal rate with a range of 2–9% (Jung et al., 2015). The results also indicate that the SS has better P-adsorption capacity and adsorption efficiency compared to lightweight aggregates and bio-materials.

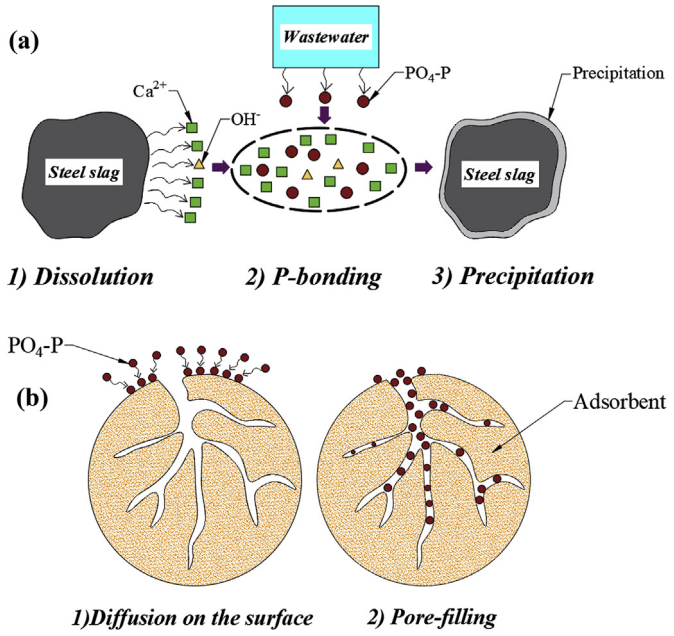

Fig. 6. The adsorption mechanism of P removal by (a) Steel slag and (b) Porous materials.

3.2.2. Adsorption isotherms

The adsorption isotherms of the materials are presented in Fig. 7. The results show that the P-adsorption capacity increases as the initial P concentration increases. However, the P-removal rate decreases with the increase in P concentration. At the initial P concentration of 700 mg/L, the maximum adsorption capacity of the SS is 9.76 mg/g, while the adsorption capacity of other materials varies from 1.45 mg/g to 1.80 mg/g. When the initial P concentration is less than 200 mg/L, the P-removal rate of the SS reaches 100%. When the initial P concentration further increases, the P-removal rate of the SS decreases. For instance, the removal rate of the SS lows down to about 55% at the initial P concentration of 700 mg/L. This is because a stepwise adsorption reaction occurs at low P concentrations due to Ca^{2+} released from SS is sufficient to

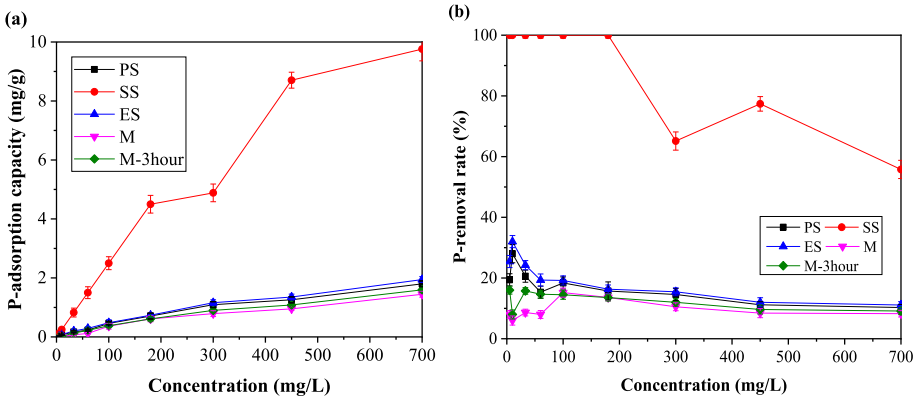

Fig. 7. The adsorption isotherms of the materials (a) P removal capacity and (b) P removal rate|(Adsorbent: 1g, P solution volume: 25 ml, Revolution per minute: 225, Time: 24 h).

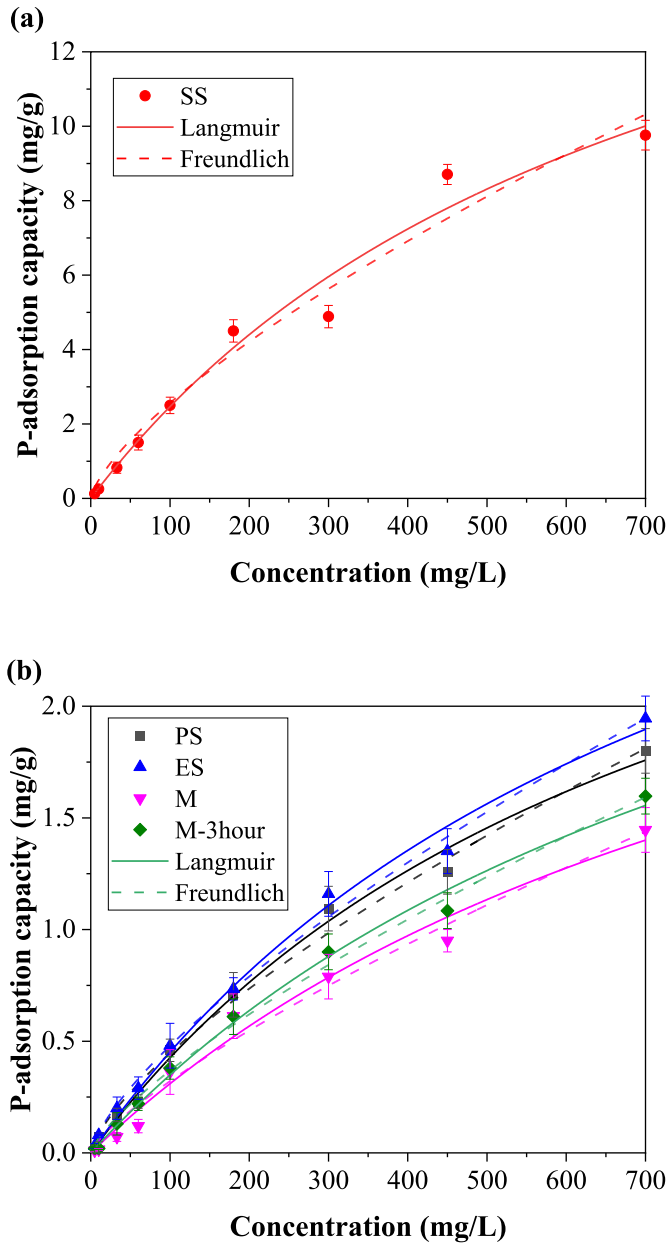

Fig. 8. The Langmuir and Freundlich isotherms of the materials.

ensure precipitation of P (Barca et al., 2012), while the precipitation of Ca–P occurs at higher P concentrations with the adsorbed P act as a core for crystal growth (Kõiv et al., 2010; Yin et al., 2011). Nevertheless, the P-removal rate of other adsorbents is about 10%, which is significantly lower than that of the SS.

The P-adsorption isotherms are analyzed by Langmuir and Freundlich equation, respectively, as shown in Fig. 8. The Langmuir and Freundlich isotherm parameters for P-adsorption are presented in Table 4. The results show that both Langmuir and Freundlich models fitted the experimental data well with very high correlation coefficient (R^2). The estimated maximum adsorption capacity of the SS is 20.40 mg/g according to the Langmuir model. The maximum adsorption capacity of the M-3hour is very close to that of the PS. However, the extraction of P from the M and the M-3hour may more easily occur than other materials because of the low holding capacity (Jung et al., 2015). The desorption results of P will be analyzed in the later section.

Table 4
Langmuir and Freundlich isotherm parameters of the materials.

Materials	Langmuir model			Freundlich model		
	Q_m	K_L	R^2	K_F	n	R^2
PS	3.676	0.00131	0.993	0.0163	1.390	0.991
SS	20.40	0.00137	0.975	0.0951	1.398	0.968
ES	4.067	0.00125	0.993	0.0174	1.389	0.994
M	3.390	0.00101	0.982	0.0092	1.298	0.980
M-3hour	3.677	0.00105	0.994	0.0115	1.329	0.994

3.2.3. Adsorption kinetics

Kinetic studies are usually used to evaluate the relationship between reaction time and the maximum adsorption capacity (Jung et al., 2015). The adsorption rate of the adsorbent usually increases rapidly during the initial reaction time and then slowly

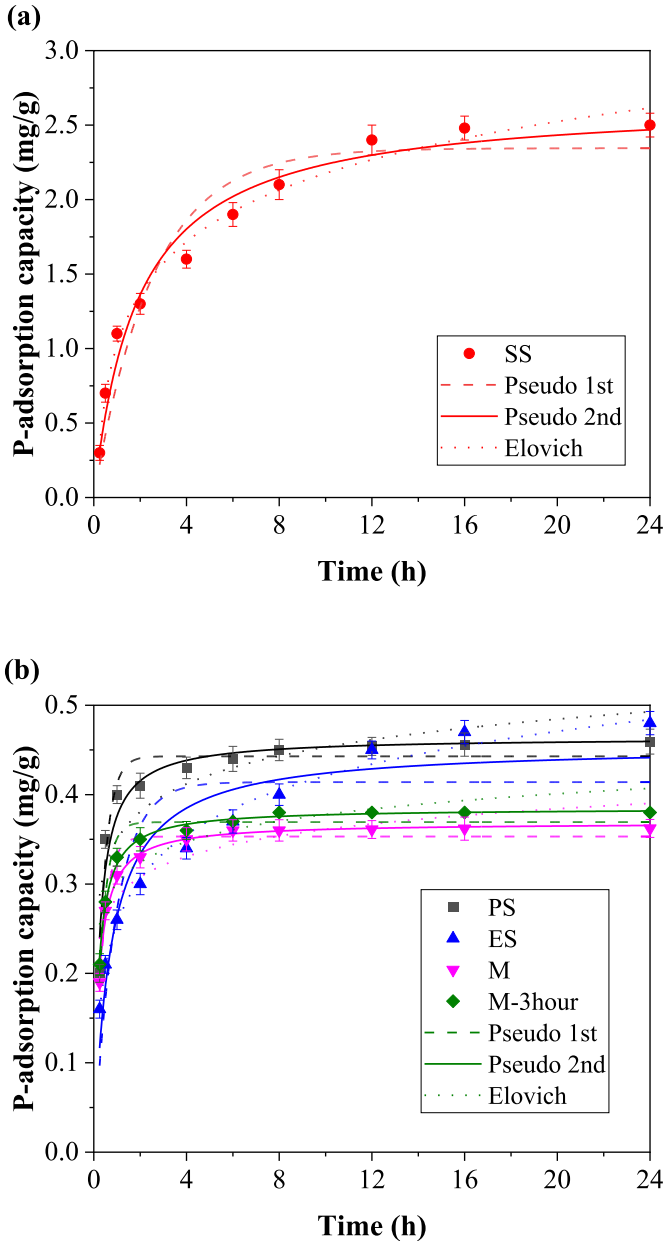

Fig. 9. The adsorption kinetics of the materials.

reaches equilibrium (Ghaedi et al., 2011). As shown in Fig. 9, the adsorption capacity of all materials increases as the reaction time increases. At the end of 2 h, the adsorption capacity of the SS only reaches 52% of the adsorption equilibrium capacity. The results also show that the adsorption rate of the SS gradually reduces with contact time increases until reaching the equilibrium after 16 h. The equilibrium time of the SS and ES are significantly longer than that of bio-materials. The varying equilibrium time may be attributed to the distinguishing characteristics of the materials, which leads to different adsorption processes and adsorption mechanisms (Yin et al., 2011).

However, the adsorption capacity of the M rapidly increases at the first 2 h, which reaches 92% of the adsorption equilibrium capacity. Previous researches reported that the adsorption capacity of the peanut shell biochar exceeds 80% of its maximum adsorption capacity within the first 4 h (Jung et al., 2015). This is attributed to a large amount of mesopores available for adsorption at the first contact time (Ghaedi et al., 2011). Moreover, the high water absorption of the M results in the mesopores being rapidly filled by the P solution in the first 2 h, then the adsorption rate rapidly decreases until reaching the equilibrium. However, the use of the SS to remove P is a slow and continuous process, indicating sufficient calcium ions gradually leach from the SS surface and then react with P for the precipitation-coagulation process. Besides, the precipitation also needs time to finish the reaction (Park et al., 2017). Therefore, as long as calcium ions are continuously released for the SS surface, the P-removal process will keep proceeding.

The experimental data are matched by the pseudo-first-order, pseudo-second-order and simple Elovich kinetic models. As shown in Fig. 9, the experimental data of P-adsorption in this study can be described well by the pseudo-second-order kinetic model. The evaluated kinetic parameters are presented in Table 5. The values of the calculated adsorption capacity are close to the experimental data according to the pseudo-second-order model. Although the Elovich model also can fit the adsorption kinetic data of the SS and the ES, the fitting quality for the M and PS are poor.

Table 5
Kinetic parameters of the materials.

Materials	Pseudo-first-order			Pseudo-second-order			Elovich		
	Q	K_1	R^2	Q	K_2	R^2	α	β	R^2
PS	0.443	2.667	0.947	0.464	9.196	0.932	0.349	0.045	0.724
SS	2.345	0.394	0.919	2.666	0.196	0.971	1.020	0.502	0.987
ES	0.414	1.065	0.741	0.455	3.025	0.894	0.256	0.072	0.989
M	0.353	2.849	0.944	0.369	12.94	0.989	0.285	0.033	0.793
M-3hour	0.369	2.990	0.937	0.385	13.29	0.992	0.301	0.033	0.810

3.2.4. Effect of pH on adsorption capacity

The high pH causes the adsorbent surface to carry a more negative charge, which significantly repulses negatively charged solutes, consequently, a high pH generally reduces the adsorption capacity of P due to the presence of repulsive forces (Park et al., 2017; Yang et al., 2006). As shown in Fig. 10, the adsorption capacity of all materials decreases by 11%–19% when the pH value increases from 3 to 11. This result is consistent with previous studies reported by Yin et al. (2011) and Bolan et al. (1986), with the maximum P-adsorption capacity appears at a pH value of around 3–4. When the pH value of the solution less than 2, the species of the P predominantly exist in H_3PO_4, which is difficult to attach to exchange sites for anion exchange. When the pH value varies from 3 to 5, the $H_2PO_4^-$, HPO_4^{2-} and PO_4^{3-} are major species for the P solution, which are available for ion exchange, especially $H_2PO_4^-$. When the pH value is more than 8, more OH^- ions are available in solution, which may compete with the species of the P for ion exchange, resulting in the reduction in the P-adsorption (Ruixia et al., 2002).

The results also show that the adsorption capacity of the SS reduces sharply when the pH values of the P solution change from acidic to alkaline. Previous studies indicate that the amount of Ca^{2+} ions leaching from the adsorbent decreases with an increase in pH value of the initial solution (Gan et al., 2009; Yin et al., 2011). Moreover, when the pH value of the solution is decreased, the

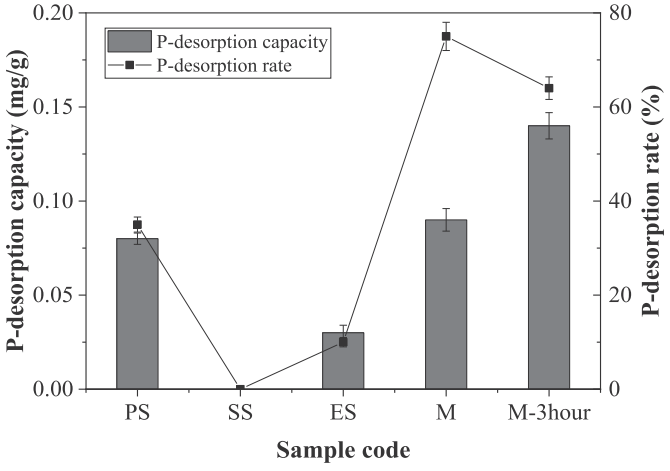

Fig. 11. The P desorption capacity and desorption rate of the material. (Adsorbent: 1g, Distilled water: 25 ml, Revolution per minute: 225, Time: 24 h).

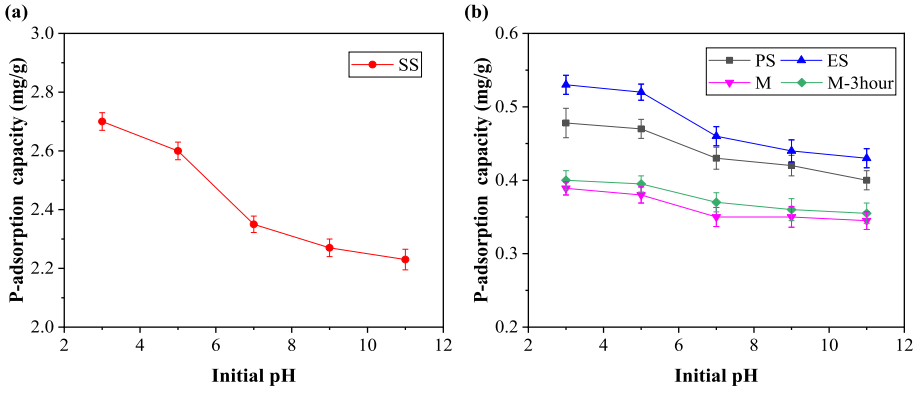

Fig. 10. Effects of pH values on the adsorption capacity(Adsorbent: 1g, P solution: 25 ml, Initial P concentration: 100 mg/L).

positively charged surface sites formed on the adsorbent promotes the P-adsorption because of the electrostatic attraction (Gan et al., 2009). An approximate 20% reduction in P adsorption capacity is observed in the calcium-rich sepiolite adsorbent (Yin et al., 2011). This is because the positively charges surface of the adsorbents is more easily combine with P in an acidic solution due to electrostatic attraction (Gan et al., 2009). Besides, the types of the P ions in solution are affected by the pH value of the solution. When the pH value varies between 3 and 7, the predominant species of P are a negatively charged $H_2PO_4^-$, which could react with the dissolved Ca^{2+} to form the precipitation by the chemical reactions as follows (Johansson and Gustafsson, 2000; Yin et al., 2011):

$$Ca^{2+} + 2H_2PO_4^- \rightarrow Ca(H_2PO_4)_2 \quad (12)$$

$$Ca(H_2PO_4)_2 + Ca^{2+} \rightarrow 2CaHPO_4 + 2H^+ \quad (13)$$

$$6CaHPO_4 + 2Ca^{2+} \rightarrow Ca_8(H_2PO_4)_6 + 4H^+ \quad (14)$$

$$Ca_8(H_2PO_4)_6 + 2Ca^{2+} + H_2O \rightarrow Ca_{10}(PO_4)_6(OH_2) + 4H^+ \quad (15)$$

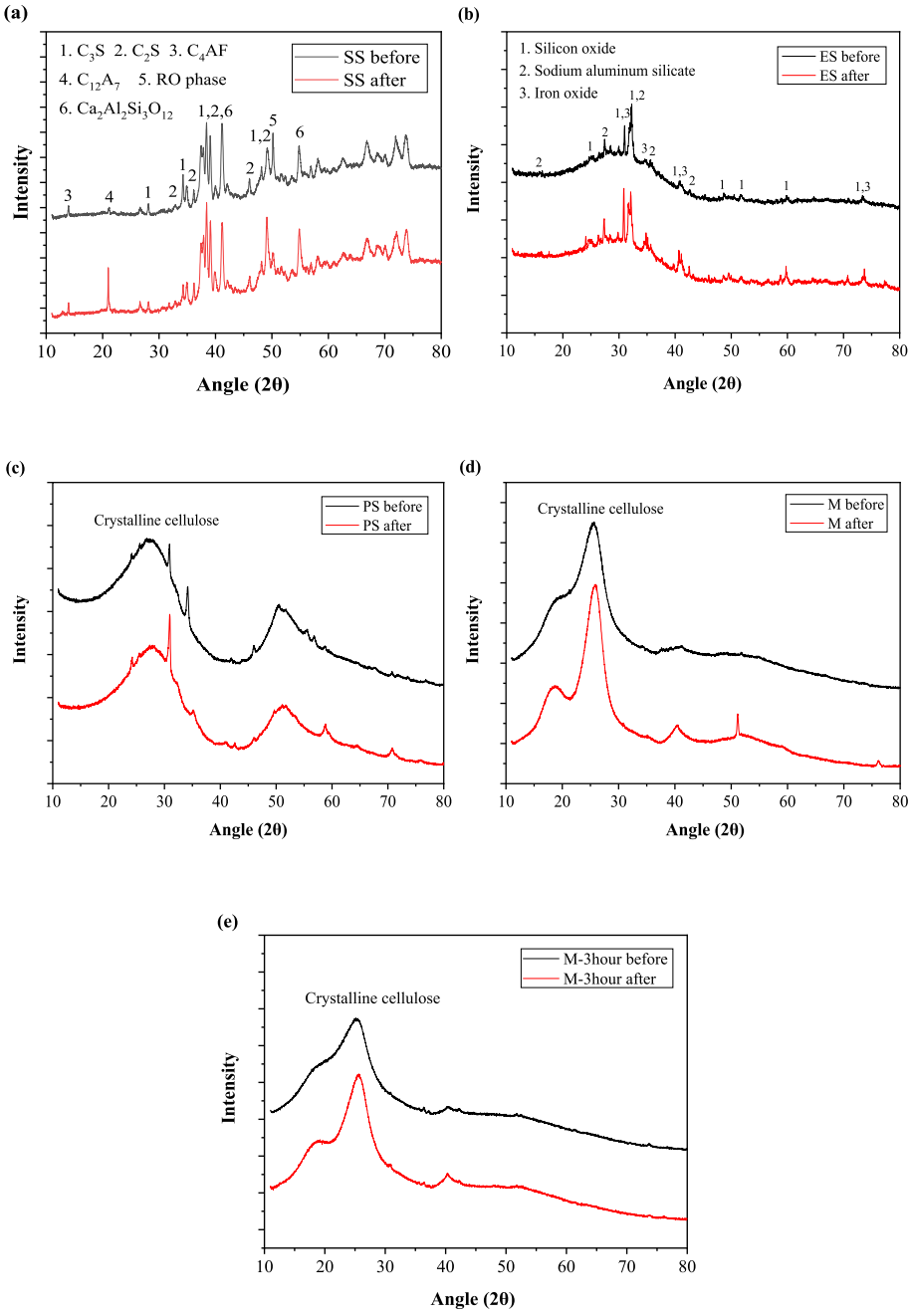

Fig. 12. The XRD patterns of the material before and after the test (a) SS, (b) ES, (c) PS, (d) M and (e) M-3 hour.

3.3. P-desorption

The P desorption capacity and desorption rate of the material are shown in Fig. 11. The results show that the P-desorption rate of the M and the M-3hour is significantly higher than that of other materials, which are more than 60%. This phenomenon indicates that the M is an unstable physical absorption, and the adsorbed P could easily be desorbed from the M, resulting in secondary pollution in the aquatic environment. It should be noted that no desorbed P is detected in the SS solution, which confirms that the combination of Ca–P is a stable precipitation process and barely desorption occurs once bonding is formed (Drizo et al., 2006; Yin et al., 2011). Therefore, the SS can be safely used as adsorptive aggregates in concrete for P-removal from water and no secondary pollution occurs.

3.4. Characterization of the adsorbents after the test

3.4.1. Mineralogical phase analysis

The XRD patterns of the material before and after the test are presented in Fig. 12. The main mineral components of the SS are $3CaO \cdot SiO_2$ (C_3S), $2CaO \cdot SiO_2$ (C_2S) and RO (Fe_2O_3, MgO and MnO) (Wang and Yan, 2010), as shown in Fig. 12a. After the P-adsorption, the diffraction peaks corresponding to C_3C and C_2S mineral phases of the SS are decreased, especially at about 35° diffraction angle compared to the pattern before adsorption, which can be explained by the hydrolysis of calcium-containing oxides (Han et al., 2015). This phenomenon indicates that the calcium-containing oxides are involved in the adsorption of P, which leads to the better adsorption capacity of the SS than other materials. The crystallized structure of the ES is characterized as silicon oxide, sodium aluminium silicate and iron oxide. Metal elements such as iron and aluminium also contributed to the P-adsorption (Zhao et al., 2007).

Similar to other bio-materials such as wood, soybean, bamboo, etc., the structure of the PS is crystalline cellulose and a distinct peak appears near the diffraction between 25° and 30°. The shape of the diffraction curve of the M and M-3hour is similar to that of the PS. The M-3hour shows a wide diffraction peak compared to the M due to the heat treatment effect (Asadi Zeidabadi et al., 2018; Wu et al., 2018). PS and M are mainly composed of C and O, which account for about 90% of the total dry weight (De Jong et al., 2003; Kaynak et al., 2005). They cannot react with P to form a new crystal

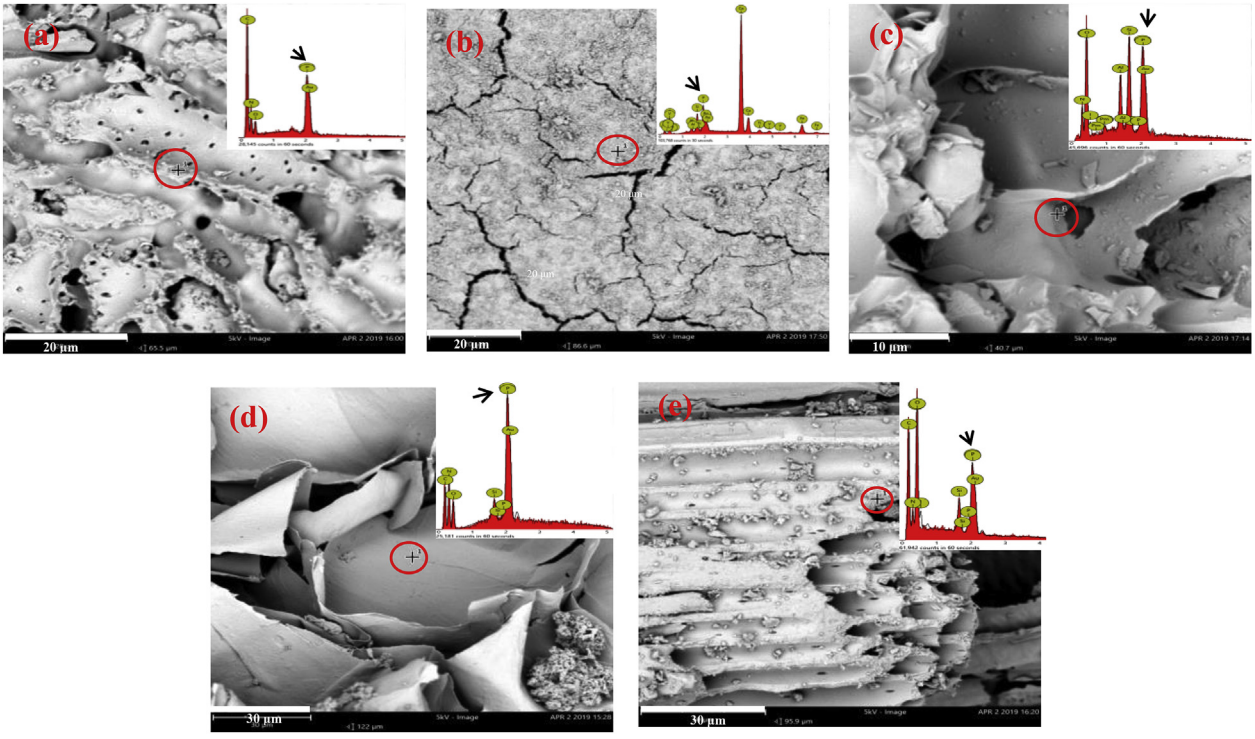

Fig. 13. The SEM images and EDS analysis of the material after adsorption test (a) PS, (b) SS, (c) ES, (d) M and (e) M-3hour.

Table 6
The elemental content obtained by SEM-EDS analysis.

Element symbol	Elemental content of samples									
	PS		SS		ES		M		M-3 hour	
	Atomic Conc.	Weight Conc.	Atomic Conc.	Weight Conc.	Atomic Conc.	Weight Conc.	Atomic Conc.	Weight Conc.	Atomic Conc.	Weight Conc.
Au	42.89	91.71	39.68	79.29	51.08	90.32	62.95	95.67	40.34	89.22
C	40.77	5.51	–	–	–	–	12.07	1.12	29.44	3.97
N	11.19	1.86	–	–	11.55	1.45	16.84	1.82	6.82	1.07
O	2.85	0.50	15.52	2.52	13.39	1.92	4.31	0.53	15.55	2.79
Si	–	–	2.81	0.80	14.95	3.77	2.63	0.57	4.89	1.54
Ca	–	–	31.93	12.98	–	–	–	–	–	–
P	2.3	0.42	3.88	1.22	0.94	0.26	1.21	0.29	2.60	0.90

structure. Therefore, the changes in the peaks of the M and the M-3hour after P-adsorption near the diffraction angle of 18° and 40° are caused by the amorphous P on the surface or micropores of the material (Han et al., 2015).

3.4.2. SEM-EDS analyses

The SEM images and the EDS analyses of the material after P adsorption are shown in Fig. 13. The results show that several small spots are selected and analyzed on the surface of other materials (Fig. 13) and the distributed crystalline substance is observed on the M-3hour surface, as shown in Fig. 13e. The finely distributed P crystals are observed on the surface of furnace slag by EDS analysis, which is the precipitate of Ca/P/O. The same phenomenon is also observed in other materials, such as furnace slag (Park et al., 2017), oil-shale ash(Kaasik et al., 2008), sepiolite (Yin et al., 2011), namely suspended Ca–P precipitation formed on the surface of the adsorbent after P-adsorption. In this study, the strong peak of P is observed in all EDS spectra and the P is detected on the surface of all materials. A higher Ca and P content is detected on the surface of the SS, as shown in Table 6. The results indicate that the surface structure of the SS has no significant effect on the P-adsorption, the chemical adsorption is predominant to the SS for P adsorption due to the dissolution of calcium and precipitation of hydroxyapatite (Barca et al., 2012).

3.5. Low-cost materials used for P-adsorption

The low-cost materials used for P-adsorption including industrial by-products, synthetic materials, natural and bio-based materials are presented in Table 7. The results indicate that the SS generally has better P adsorption capacity than most of the bio-materials and unmodified natural materials, but lower than synthetic materials and modified natural materials. However, although the synthetic materials have higher adsorption capacity, they are powdery and are not suitable for application as aggregates in concrete. Similar to the modified natural aggregates coated with chemical solvents, the use of synthetic materials in concrete may lead to secondary pollution of the water environment (Sabhi and Kiwi, 2001).

Bio-based activated carbon such as bamboo, juniper fibre and date palm fibre has been widely used as adsorbents in water treatment, but the adsorption capacity of bio-materials is relatively limited compared to the SS. Besides, they are generally elongated and flaky particle, and their application as aggregates results in a weak interfacial transition zone and low mechanical properties of concrete (Wu et al., 2018). However, the granular SS has a much higher strength than other biological materials, which is feasible to be directly used as aggregates in concrete. Therefore, SS can be considered as an effective adsorptive aggregate to replace the non-adsorptive aggregate for increasing the P-removal of adsorptive concrete because of the excellent mechanical and adsorption properties.

4. Conclusions

In this study, the adsorption characteristics of the industrial by-product (SS), lightweight aggregates (ES) and bio-materials (PS and M) under identical experimental conditions are evaluated for potential applications in highly adsorptive concrete. The effects of parameters such as the initial concentrations of P, reaction time and pH value on adsorption capacity and efficiency of P are investigated using an IC analyzer. The adsorption mechanism of P is discussed based on BET, ICP-AES, XRD and SEM-EDS analyses. The following conclusions can be drawn:

(1) The SS exhibits high P adsorption capacity and adsorption efficiency compared to lightweight aggregates and bio-materials. The maximum adsorption capacity of the SS is 20.40 mg/g according to the Langmuir model. The adsorption kinetics are fitted well by the pseudo-second-order kinetic model. Moreover, the SS has very low P-desorption, which indicates that the SS can be safely used as adsorptive aggregates in concrete for P removal and no P-desorption occurs.

(2) The adsorption mechanism of the SS is attributed to the Ca^{2+} leached from the SS surface, which can react with P to form Ca–P precipitate. Moreover, the chemisorption process is continuous and stable, indicating sufficient calcium ions gradually leach from the SS surface and then react with P for the precipitation-coagulation process. It is suggested that the

Table 7
Low-cost materials used for P-adsorption.

Materials	Particle size (mm)	Adsorption capacity (mg/g)	Initial concentration (mg/L)	Agitation mode (rpm)	Contact time (h)	P removal (%)
Industrial materials						
Steel slag (SS) in this study	1–2	9.76	700	225	24	55
Basic oxygen furnace slag (Park et al., 2017)	0.8–2.3	2.81	–	4000	24	–
Steel slag (Barca et al., 2012)	5–10	2.49	100	125	24	>90
Furnace slag (Xu et al., 2006)	<5	8.89	400–600	200	24	–
Fly ash (Agyei et al., 2002)	<0.3	32	400	120	16	–
Coal ash (Drizo et al., 1999)	<2.8	0.86	35–45	–	12	–
Synthetic materials						
Fe–Cu binary oxide (Li et al., 2014)	Powder	35.2	30	160	24	–
Aluminium oxide hydroxide (Tanada et al., 2003)	Powder	35	8	600	4	–
Modified iron hydroxide (Seida and Nakano, 2002)	Powder	28.8	–	–	24	–
Natural materials						
Modified palygorskite (Gan et al., 2009)	<0.15	42	1000	200	24	–
Modified sepiolite (Yin et al., 2011)	<0.15	32	100	160	24	86
Quartz sand (Han et al., 2009)	0.5–2	0.30	25	140	24	87.7
Bio-based materials						
Peanut shell (Jung et al., 2015)	Powder	3.8	5	200	48	61.3
Bamboo (Ramola et al., 2014)	Powder	<2.5	6.5	200	24	42.15
Juniper fiber (Han et al., 2005)	Powder	<0.5	10	150	24	–
Date palm fiber (Riahi et al., 2009)	Powder	1.75	50	200	2	–

steel slag can function as effective adsorptive aggregates for the manufacture of high adsorptive concrete.

(3) Heat treatment can be used to increase the adsorption capacity of the M. The adsorption capacity of the M after 3-h heat treatment increases from 3.39 mg/g to 3.68 mg/g due to the change in pore structure characteristics. The P-adsorption of the M and PS follows a physical adsorption mechanism due to the well-developed mesoporous structure and high specific surface area. However, the high water absorption of the M results in the rapid P-adsorption in the initial reaction time and also leads to the high P-desorption.

CRediT authorship contribution statement

Fan Wu: Methodology, Investigation, Data curation, Formal analysis, Validation, Writing - original draft. **Qingliang Yu:** Conceptualization, Supervision, Project administration, Writing - review & editing. **F. Gauvin:** Writing - review & editing. **H.J.H. Brouwers:** Supervision, Project administration, Writing - review & editing. **Changwu Liu:** Supervision.

Declaration of competing interest

The authors declare that they have no known competing financial interests or personal relationships that could have appeared to influence the work reported in this paper.

Acknowledgement

This work is funded by the Graduate Student's Research and Innovation Fund of Sichuan University (Grant No. 2018YJSY091), and the China Scholarship Council (CSC) Fund (Grant No. 201806240037) and Eindhoven University of Technology. The authors gratefully thank Ing. Anneke Delsing for the support with the chemical test analysis. NNRGY (The Netherlands), ENCI (The Netherlands) and TATA steel (The Netherlands) are thanked for the materials supply.

References

Agyei, N.M., Strydom, C.A., Potgieter, J.H., 2002. The removal of phosphate ions from aqueous solution by fly ash, slag, ordinary Portland cement and related blends. Cement Concr. Res. 32, 1889–1897. https://doi.org/10.1016/S0008-8846(02)00888-8.

Asadi Zeidabadi, Z., Bakhtiari, S., Abbaslou, H., Ghanizadeh, A.R., 2018. Synthesis, characterization and evaluation of biochar from agricultural waste biomass for use in building materials. Construct. Build. Mater. 181, 301–308. https://doi.org/10.1016/j.conbuildmat.2018.05.271.

Bannerman, R.T., Owens, D.W., Dodds, R.B., Hornewer, N.J., 1993. Sources of pollutants in Wisconsin stormwater. Water Sci. Technol. 28, 241–259.

Barca, C., Gérente, C., Meyer, D., Chazarenc, F., Andrès, Y., 2012. Phosphate removal from synthetic and real wastewater using steel slags produced in Europe. Water Res. 46, 2376–2384. https://doi.org/10.1016/j.watres.2012.02.012.

Barca, C., Meyer, D., Liira, M., Drissen, P., Comeau, Y., Andrès, Y., Chazarenc, F., 2014. Steel slag filters to upgrade phosphorus removal in small wastewater treatment plants: removal mechanisms and performance. Ecol. Eng. 68, 214–222. https://doi.org/10.1016/j.ecoleng.2014.03.065.

Bolan, N.S., Syers, J.K., Tillman, R.W., 1986. Ionic strength effects on surface charge and adsorption of phosphate and sulphate by soils. J. Soil Sci. 37, 379–388.

Bowden, L.I., Jarvis, A.P., Younger, P.L., Johnson, K.L., 2009. Phosphorus removal from waste waters using basic oxygen steel slag. Environ. Sci. Technol. 43, 2476–2481. https://doi.org/10.1021/es801626d.

Dastgheib, S.A., Rockstraw, D.A., 2001. Pecan shell activated carbon: synthesis, characterization, and application for the removal of copper from aqueous solution. Carbon N. Y. 39, 1849–1855. https://doi.org/10.1016/S0008-6223(00)00315-8.

De Jong, W., Pirone, A., Wójtowicz, M.A., 2003. Pyrolysis of Miscanthus Giganteus and wood pellets: TG-FTIR analysis and reaction kinetics. Fuel 82, 1139–1147. https://doi.org/10.1016/S0016-2361(02)00419-2.

Drizo, A., Frost, C.A., Grace, J., Smith, K.A., 1999. Physico-chemical screening of phosphate-removing substrates for use in constructed wetland systems. Water Res. 33, 3595–3602. https://doi.org/10.1016/S0043-1354(99)00082-2.

Drizo, A., Forget, C., Chapuis, R.P., Comeau, Y., 2006. Phosphorus removal by electric arc furnace steel slag and serpentinite. Water Res. 40, 1547–1554. https://doi.org/10.1016/j.watres.2006.02.001.

Forbes, M.G., Dickson, K.R., Golden, T.D., Hudak, P., Doyle, R.D., 2004. Dissolved phosphorus retention of light-weight expanded shale and masonry sand used in subsurface flow treatment wetlands. Environ. Sci. Technol. 38, 892–898. https://doi.org/10.1021/es034341z.

Gan, F., Zhou, J., Wang, H., Du, C., Chen, X., 2009. Removal of phosphate from aqueous solution by thermally treated natural palygorskite. Water Res. 43, 2907–2915. https://doi.org/10.1016/j.watres.2009.03.051.

Ghaedi, M., Hassanzadeh, A., Kokhdan, S.N., 2011. Multiwalled carbon nanotubes as adsorbents for the kinetic and equilibrium study of the removal of Alizarin red S and morin. J. Chem. Eng. Data 56, 2511–2520. https://doi.org/10.1021/je2000414.

Gizińska-Górna, M., Pytka, A., Listosz, A., 2017. Analysis of the influence of a hybrid constructed wetland wastewater treatment plant on the water quality of the receiver. Annu. Set Environ. Prot. 19, 370–393.

Guo, C., Li, H., Fang, F., Ji, Y., Xing, Y., Fan, Y., Liu, Y., 2018. Study on distribution of phosphorus fractions and adsorption-desorption characteristics in surface sediments of the Yellow River by molybdenum antimony spectrophotometry. Spectrosc. Spectr. Anal. 38, 218–223. https://doi.org/10.3964/j.issn.1000-0593(2018)01-0218-06.

Han, J.S., Min, S.H., Kim, Y.K., 2005. Removal of phosphorus using AMD-treated lignocellulosic material. For. Prod. J. 55, 48–53.

Han, Y., Park, S., Lee, C., Park, J., Choi, N., Kim, S., 2009. Phosphate removal from aqueous solution by aluminum. Environ. Educ. Res. 14, 164–169.

Han, C., Wang, Z., Yang, H., Xue, X., 2015. Removal kinetics of phosphorus from synthetic wastewater using basic oxygen furnace slag. J. Environ. Sci. (China) 30, 21–29. https://doi.org/10.1016/j.jes.2014.11.003.

Haselbach, L., Poor, C., Tilson, J., 2014. Dissolved zinc and copper retention from stormwater runoff in ordinary portland cement pervious concrete. Construct. Build. Mater. 53, 652–657. https://doi.org/10.1016/j.conbuildmat.2013.12.013.

Helyar, K.R., Munns, D.N., Burau, R.G., 1976a. Adsorption of phosphate by gibbsite I. effects of neutral chloride salts of calcium, magnesium, sodium, and potassium. J. Soil Sci. 27, 307–314.

Helyar, K.R., Munns, D.N., Burau, R.G., 1976b. Adsorption of phosphate by gibbsite II. formation of a surface complex involving divalent cations. J. Soil Sci. 27, 315–323.

Jiang, C., Jia, L., Zhang, B., He, Y., Kirumba, G., 2014. Comparison of quartz sand, anthracite, shale and biological ceramsite for adsorptive removal of phosphorus from aqueous solution. J. Environ. Sci. (China) 26, 466–477. https://doi.org/10.1016/S1001-0742(13)60410-6.

Jo, M., Soto, L., Arocho, M., St John, J., Hwang, S., 2015. Optimum mix design of fly ash geopolymer paste and its use in pervious concrete for removal of fecal coliforms and phosphorus in water. Construct. Build. Mater. 93, 1097–1104. https://doi.org/10.1016/j.conbuildmat.2015.05.034.

Johansson, L., Gustafsson, J.P., 2000. Phosphate removal using blast furnace slags and opoka-mechanisms. Water Res. 34, 259–265. https://doi.org/10.1016/S0043-1354(99)00135-9.

Jung, K.W., Hwang, M.J., Ahn, K.H., Ok, Y.S., 2015. Kinetic study on phosphate removal from aqueous solution by biochar derived from peanut shell as renewable adsorptive media. Int. J. Environ. Sci. Technol. 12, 3363–3372. https://doi.org/10.1007/s13762-015-0766-5.

Kaasik, A., Vohla, C., Mõtlep, R., Mander, Ü., Kirsimäe, K., 2008. Hydrated calcareous oil-shale ash as potential filter media for phosphorus removal in constructed wetlands. Water Res. 42, 1315–1323. https://doi.org/10.1016/j.watres.2007.10.002.

Kaynak, B., Topal, H., Atimtay, A.T., 2005. Peach and apricot stone combustion in a bubbling fluidized bed. Fuel Process. Technol. 86, 1175–1193. https://doi.org/10.1016/j.fuproc.2004.12.007.

Kõiv, M., Liira, M., Mander, Ü., Mõtlep, R., Vohla, C., Kirsimäe, K., 2010. Phosphorus removal using Ca-rich hydrated oil shale ash as filter material - the effect of different phosphorus loadings and wastewater compositions. Water Res. 44, 5232–5239. https://doi.org/10.1016/j.watres.2010.06.044.

Lee, H.W., Cho, H.J., Yim, J.H., Kim, J.M., Jeon, J.K., Sohn, J.M., Yoo, K.S., Kim, S.S., Park, Y.K., 2011. Removal of Cu(II)-ion over amine-functionalized mesoporous silica materials. J. Ind. Eng. Chem. 17, 504–509. https://doi.org/10.1016/j.jiec.2010.09.022.

Lehr, J.J., Van Wesemael, J.C., 1952. The influence of neutral salts on the solubility of soil phosphate with special reference to the effect of the nitrates of sodium and calcium. J. Soil Sci. 3, 125–135.

Li, G., Gao, S., Zhang, G., Zhang, X., 2014. Enhanced adsorption of phosphate from aqueous solution by nanostructured iron(III)-copper(II) binary oxides. Chem. Eng. J. 235, 124–131. https://doi.org/10.1016/j.cej.2013.09.021.

Lin, G., Jiang, J., Wu, K., Cai, Z., Sun, K., Lu, X., 2016. Pore structure analysis and methane adsorption of self-form granular activated carbon by phosphoric acid activation. Chem. Ind. For. Prod. 36, 101–106. https://doi.org/10.3969/j.issn.0253-2417.2016.05.015.

Luo, Y., Zhao, L., Meng, H., Xiang, X., Zhao, X., Li, G., Lin, Q., 2013. Physio-chemical characterization of biochars pyrolyzed from miscanthus under two different temperatures. Trans. Chin. Soc. Agric. Eng. 29, 208–217.

Naghipour, D., Taghavi, K., Jaafari, J., Mahdavi, Y., Ghozikali, M.G., Ameri, R., Jamshidi, A., 2015. Statistical modeling and optimization of the phosphorus biosorption by modified Lemna minor from aqueous solution using response

surface methodology (RSM). Desalin. Water Treat. 3994, 1–12. https://doi.org/10.1080/19443994.2015.1100555.
Nkansah, M.A., Christy, A.A., Barth, T., Francis, G.W., 2012. The use of lightweight expanded clay aggregate (LECA) as sorbent for PAHs removal from water. J. Hazard Mater. 217–218, 360–365. https://doi.org/10.1016/j.jhazmat.2012.03.038.
Osman, A.I., Ahmed, A.T., Johnston, C.R., Rooney, D.W., 2018. Physicochemical characterization of miscanthus and its application in heavy metals removal from wastewaters. Environ. Prog. Sustain. Energy 37, 1058–1067. https://doi.org/10.1002/ep.12783.
Park, J.H., Wang, J.J., Kim, S.H., Cho, J.S., Kang, S.W., Delaune, R.D., Seo, D.C., 2017a. Phosphate removal in constructed wetland with rapid cooled basic oxygen furnace slag. Chem. Eng. J. 327, 713–724. https://doi.org/10.1016/j.cej.2017.06.155.
Ramola, S., Mishra, T., Rana, G., Srivastava, R.K., 2014. Characterization and pollutant removal efficiency of biochar derived from baggage, bamboo and tyre. Environ. Monit. Assess. 186, 9023–9039. https://doi.org/10.1007/s10661-014-4062-5.
Riahi, K., Thayer, B.Ben, Mammou, A.Ben, Jaafoura, M.H., 2009. Biosorption characteristics of phosphates from aqueous solution onto Phoenix dactylifera L. date palm fibers. J. Hazard Mater. 170, 511–519. https://doi.org/10.1016/j.jhazmat.2009.05.004.
Rizzo, G., Rizzo, G.F., 2015. Use of Biochar Geostructures for Urban Stormwater Water Cleanup USE of BIOCHAR GEOSTRUCTURES for URBAN STORMWATER WATER CLEANUP Courses ENG4111 and ENG4112 Research Project towards the Degree of Bachelor of Engineering (Civil Engineering) 1–90.
Rouquerol, J., Rouquerol, F., Llewellyn, P., Maurin, G., Sing, K.S.W., 2013. Adsorption by Powders and Porous Solids: Principles, Methodology and Applications. Academic press.
Ruixia, L., Jinlong, G., Hongxiao, T., 2002. Adsorption of fluoride, phosphate, and arsenate ions on a new type of ion exchange fiber. J. Colloid Interface Sci. 248, 268–274. https://doi.org/10.1006/jcis.2002.8260.
Sabhi, S., Kiwi, J., 2001. Degradation of 2,4-dichlorophenol by immobilized iron catalysts. Water Res. 35 https://doi.org/10.1016/S0043-1354(00)00460-7, 1994–2002.
Sayari, A., Hamoudi, S., Yang, Y., 2005. Applications of pore-expanded mesoporous silica. 1. Removal of heavy metal cations and organic pollutants from wastewater. Chem. Mater. 17, 212–216. https://doi.org/10.1021/cm048393e.
Seida, Y., Nakano, Y., 2002. Removal of phosphate by layered double hydroxides containing iron. Water Res. 36, 1306–1312. https://doi.org/10.1016/S0043-1354(01)00340-2.
Shabalala, A.N., Ekolu, S.O., Diop, S., Solomon, F., 2017. Pervious concrete reactive barrier for removal of heavy metals from acid mine drainage – column study. J. Hazard Mater. 323, 641–653. https://doi.org/10.1016/j.jhazmat.2016.10.027.
Shi, C., 2004. Steel slag - its production, processing, characteristics, and cementitious properties. J. Mater. Civ. Eng. 16, 230–236. https://doi.org/10.1061/(ASCE)0899-1561(2004)16:3(230).
Shilton, A.N., Elmetri, I., Drizo, A., Pratt, S., Haverkamp, R.G., Bilby, S.C., 2006. Phosphorus removal by an 'active' slag filter—a decade of full scale experience. Water Res. 40, 113–118. https://doi.org/10.1016/J.WATRES.2005.11.002.
Tan, X., Liu, Y., Zeng, G., Wang, X., Hu, X., Gu, Y., Yang, Z., 2015. Application of biochar for the removal of pollutants from aqueous solutions. Chemosphere 125, 70–85. https://doi.org/10.1016/j.chemosphere.2014.12.058.
Tanada, S., Kabayama, M., Kawasaki, N., Sakiyama, T., Nakamura, T., Araki, M., Tamura, T., 2003. Removal of phosphate by aluminum oxide hydroxide. J. Colloid Interface Sci. 257, 135–140. https://doi.org/10.1016/S0021-9797(02)00008-5.
Taylor, P., Safari, G.H., Zarrabi, M., Hoseini, M., Kamani, H., 2014. Desalination and Water Treatment Trends of natural and acid-engineered pumice onto phosphorus ions in aquatic environment : adsorbent preparation , characterization , and kinetic and equilibrium modeling. Desalin. Water Treat. 37–41. https://doi.org/10.1080/19443994.2014.915385.
Vázquez-Rivera, N.I., Soto-Pérez, L., St John, J.N., Molina-Bas, O.I., Hwang, S.S., 2015. Optimization of pervious concrete containing fly ash and iron oxide nanoparticles and its application for phosphorus removal. Construct. Build. Mater. 93, 22–28. https://doi.org/10.1016/j.conbuildmat.2015.05.110.
Wang, Q., Yan, P., 2010. Hydration properties of basic oxygen furnace steel slag. Construct. Build. Mater. 24, 1134–1140. https://doi.org/10.1016/j.conbuildmat.2009.12.028.
Wang, S., Xu, Y., Norbu, N., Wang, Z., 2018. Remediation of biochar on heavy metal polluted soils. IOP Conf. Ser. Earth Environ. Sci. 108 https://doi.org/10.1088/1755-1315/108/4/042113.
Wu, F., Liu, C., Zhang, L., Lu, Y., Ma, Y., 2018. Comparative study of carbonized peach shell and carbonized apricot shell to improve the performance of lightweight concrete. Construct. Build. Mater. 188, 758–771. https://doi.org/10.1016/j.conbuildmat.2018.08.094.
Xu, D., Xu, J., Wu, J., Muhammad, A., 2006. Studies on the phosphorus sorption capacity of substrates used in constructed wetland systems. Chemosphere 63, 344–352. https://doi.org/10.1016/j.chemosphere.2005.08.036.
Yaghoobi, S., Sharafie, K., Biglari, H., 2017. Mucilage of Plantago ovata as natural coagulation – flocculation aid in an electrocoagulation process for phosphate removal from aqueous environments. Desalin. Water Treat. 99, 21475. https://doi.org/10.5004/dwt.2017.21475.
Yang, Y., Zhao, Y.Q., Babatunde, A.O., Wang, L., Ren, Y.X., Han, Y., 2006. Characteristics and mechanisms of phosphate adsorption on dewatered alum sludge. Separ. Purif. Technol. 51, 193–200. https://doi.org/10.1016/j.seppur.2006.01.013.
Yin, H., Yun, Y., Zhang, Y., Fan, C., 2011. Phosphate removal from wastewaters by a naturally occurring, calcium-rich sepiolite. J. Hazard Mater. 198, 362–369. https://doi.org/10.1016/j.jhazmat.2011.10.072.
Zhang, Y., Li, G., 2011. Principle and Application of Activated Carbon-Nanofiltration in Treatment of Micro-Polluted Source Water, Science PrCess. Science Press, Beijing.
Zhao, G., Zhou, Q., Li, X., 2007. Adsorption of phosphorus from aqueous solution on steel converter slags. J. Tongji Univ. (Natural Sci. 35, 1510–1514.
Zhu, H., Yu, T., Wei, D., Wang, X., He, T., Wu, Y., Qi, J., 2018. The adsorption of phosphorus in simulated wastewater by immersing and annealing modified attapulgite. Res. Environ. Sci. 31, 765–773.